International Journal of Solids and Structures 47 (2010) 827–836

Contents lists available at ScienceDirect

International Journal of Solids and Structures

journal homepage: www.elsevier.com/locate/ijsolstr

Elastoplastic modeling of circular fiber-reinforced ductile matrix composites considering a finite RVE

B.R. Kim, H.K. Lee *

Department of Civil and Environmental Engineering, Korea Advanced Institute of Science and Technology, Guseong-dong, Yuseong-gu, Daejeon 305-701, Republic of Korea

ARTICLE INFO

Article history:
Received 13 November 2008
Received in revised form 23 March 2009
Available online 27 November 2009

Keywords:
Metal-matrix composites (MMCs)
Debonding
Elastoplasticity
Micromechancis
Debonding
Finite RVE

ABSTRACT

A micromechanical elastoplastic damage model considering a finite RVE is proposed to predict the overall elastoplastic damage behavior of circular fiber-reinforced ductile (matrix) composites. The constitutive damage model proposed in our preceding work (Kim and Lee, 2009) considering a finite Eshelby's tensor (Li et al., 2005; Wang et al., 2005) is extended to accommodate the elastoplastic behavior of the composites. On the basis of the exterior-point Eshelby's tensor for circular inclusions and the ensemble-averaged effective yield criterion, a micromechanical framework for predicting the effective elastoplastic damage behavior of ductile composites is derived. A series of numerical simulations are carried out to illustrate stress–strain response of the proposed micromechanical framework and to examine the influence of a Weibull parameter on the elastoplastic behavior of the composites. Furthermore, comparisons between the present predictions and experimental data available in the literature are made to further assess the predictive capability of the proposed model.

1. Introduction

Fiber-reinforced composites made of high-modulus fibers and relatively ductile matrix have been widely used as advanced materials in aerospace, automotive, and infrastructure applications. Fiber-reinforced composites demonstrate a great potential for many applications due to their superior mechanical properties in the fiber direction, but the transverse behavior of the fiber-reinforced composites is shown to be relatively weak (Oleszkiewicz and Łodygowski, 2006). The most likely damage mechanism of fiber-reinforced composites under transverse tensile loading can be characterized by both an initial damage resulting from partial fiber debonding and the plastic deformation by plastic yielding (Oleszkiewicz and Łodygowski, 2006; Ju and Ko, 2008). Thus, a model capable of predicting the evolutionary fiber debonding and plasticity is needed for an accurate estimation of the behavior of fiber-reinforced ductile composites.

Although a variety of research on various mechanical properties and geometries of composites have been conducted, most of them emphasize the elastic range (Huang, 1971). Plasticity has been studies recently to understand and model the ductility and material nonlinearity of ductile composites (Khan et al., 2007). Refer to Hill (1950), Lubliner (1990), Khan and Huang (1995), Simo (1998) and Simo and Hughes (1998) for detailed descriptions of various plasticity theories and models (Moreo et al., 2007). Many studies have also focused on the interfacial debonding between fibers and the matrix (Whitehouse and Clyne, 1993; Meraghni et al., 1996; Bansal and Eldridge, 1999; Chiang, 2001; Caporale et al., 2006; Li and Ghosh, 2007).

The (classical) Eshelby's inclusion solution (Eshelby, 1957, 1959) based on the assumption that an inclusion is embedded in an unbounded infinite domain has been widely employed to analyze the behavior of heterogeneous materials. Refer to Ju and Chen (1994), Ju and Tseng (1996), Ju and Lee (2000, 2001), Ju and Sun (2001), Ju and Zhang (2001), Lee and Simunovic (2001) and Lee and Pyo (2008) for Eshelby's inclusion solution based micromechanical elastoplastic composite modeling. The classical Eshelby's tensor approach could be a good approximation if the size of an inclusion is small compared to the size of the representative volume element (RVE). However, the size of every RVE, in fact, is finite and the Eshelby's tensor needs to be dependent on the size of the inclusion (Li et al., 2005; Wang et al., 2005). Li et al. (2005) and Wang et al. (2005) proposed a finite Eshelby's tensor for circular inclusions to solve the limitation of the (classical) Eshelby's inclusion solution. Kim and Lee (2009) incorporated the finite Eshelby's tensor into formulations of micromechanical framework and derived the effective elastic moduli of circular fiber-reinforced composites.

The present study aims to develop a micromechanical elastoplastic damage model considering a finite RVE for predicting the overall elastoplastic damage behavior of circular fiber-reinforced ductile composites. The constitutive damage model proposed in our preceding work (Kim and Lee, 2009) considering a finite

* Corresponding author. Tel.: +82 42 869 3623.
E-mail address: leeh@kaist.ac.kr (H.K. Lee).

0020-7683/$ - see front matter © 2009 Elsevier Ltd. All rights reserved.
doi:10.1016/j.ijsolstr.2009.11.015

Eshelby's tensor (Li et al., 2005; Wang et al., 2005) is extended in the present study to accommodate the elastoplastic behavior of the composites. The micromechanical framework for predicting the effective elastoplastic damage response of ductile composites is derived based on the exterior-point Eshelby's tensor for circular inclusions and the ensemble-averaged effective yield criterion. Numerical simulations including a parametric analysis are carried out to illustrate the stress–strain response of the proposed micromechanical framework and to examine the model parameter sensitivity to the proposed model. Moreover, the present predictions are compared with experimental data available in the literatures to verify the proposed elastoplastic model.

2. Effective elastoplastic damage behavior of circular fiber-reinforced ductile composites

2.1. Overview

Let us start by considering an initially perfectly bonded two-phase composite consisting of a matrix (phase 0) and unidirectionally aligned, elastic circular fibers (phase 1). As loads or deformations increase, some initially perfectly bonded fibers are transformed to debonded fibers that are regarded as (circular) voids (phase 2) within the present framework. The schematic of the composite is shown in Fig. 1, where the fiber orientation of the composite is assumed to be random in the 1–2 plane. With the help of the finite Eshelby's tensor proposed by Li et al. (2005) and Wang et al. (2005) for both perfectly bonded circular fibers and circular voids, a two-dimensional (2D) micromechanics-based constitutive model considering a finite RVE for the three-phase, circular fiber-reinforced composite was explicitly derived in our preceding work (Kim and Lee, 2009) as follows.

$$\mathbf{C}_* = \lambda^*\delta_{ij}\delta_{kl} + \mu^*(\delta_{ik}\delta_{jl} + \delta_{il}\delta_{jk}) \tag{1}$$

where the Lame constants λ^* and μ^* for the three-phase composites and the details of the constitutive model can be found in Kim and Lee (2009).

After the evolutionary damage between circular fibers and the matrix, the debonded circular fibers may lose the load-carrying capacity and are assumed here to be completely debonded fibers (circular voids). For convenience, a two-parameter Weibull process (Weibull, 1951) is adopted as an evolutionary damage model and the average internal stress of fibers is used as the controlling factor in the Weibull process (Tohgo and Weng, 1994; Zhao and Weng, 1996, 1997; Ju and Lee, 2000). Accordingly, the current completely debonded fiber volume fraction ϕ_2 at a level of the uniaxial tensile loading (in the 1-direction) can be written as (see, e.g., Ju and Lee (2000) and Kim and Lee (2009))

$$\phi_2 = \phi P_d[(\bar{\sigma}_{11})_1] = \phi\left\{1 - exp\left[-\left(\frac{(\bar{\sigma}_{11})_1}{S_0}\right)^M\right]\right\} \tag{2}$$

where ϕ is the original fiber volume fraction, and S_0 and M are Weibull parameters. $(\bar{\sigma}_{11})_1$ is the internal stress of fibers (phase 1) in the 1-direction and the subscript $(\cdot)_1$ denotes the fiber phase. Details of the internal stresses of fibers required for the initiation of the evolutionary damage was derived in our preceding work (Kim and Lee, 2009) (see Eqs. (12)–(14) therein).

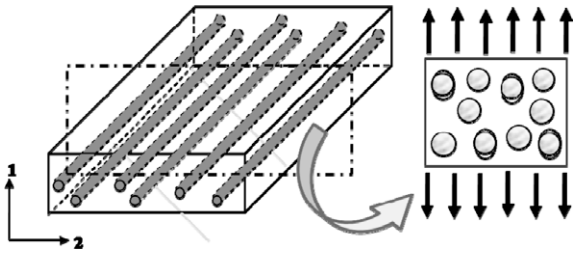

Fig. 1. The schematic of a circular fiber-reinforced composite under uniaxial tension in the transverse (1-axis) direction.

The overall elastoplastic response of the three-phase composite consisting of a ductile matrix (phase 0), perfectly bonded circular fibers (phase 1), and circular voids (phase 2) are formulated in the present study. For simplicity, the J_2-type, von-Mises yield criterion with isotropic hardening law is adopted for the matrix. Thus, the following yield criterion, which is functions of the stress $\boldsymbol{\sigma}$ and the equivalent plastic strain $\bar{e}^p$ at any point in the matrix, valids (see, e.g., Ju and Lee (2000), Ju and Zhang (2001), Lee and Simunovic (2001), and Lee and Pyo (2008)).

$$F(\boldsymbol{\sigma}, \bar{e}^p) = H(\boldsymbol{\sigma}) - K^2(\bar{e}^p) \leqslant 0 \tag{3}$$

where $K(\bar{\epsilon}^p)$ signify the isotropic hardening function of the matrix and $H(\boldsymbol{\sigma}) \equiv \boldsymbol{\sigma} : \mathbf{I}_d : \boldsymbol{\sigma}$ is the square of the deviatoric stress norm in which $\mathbf{I}_d$ denotes the deviatoric part of the fourth-rank identity tensor $\mathbf{I}$ (Ju and Lee, 2000).

According to Ju and Chen (1994), Ju and Tseng (1996), Ju and Lee (2000), Ju and Sun (2001), Ju and Zhang (2001), and Lee and Pyo (2008), the square of the current stress norm, denoted by $H(\mathbf{x}|\varpi)$, at the local point $\mathbf{x}$ determining the plastic strain in the composites for a given phase configuration ϖ is given by

$$H(\mathbf{x}|\varpi) = \begin{cases} \boldsymbol{\sigma}(\mathbf{x}|\varpi) : \mathbf{I}_d : \boldsymbol{\sigma}(\mathbf{x}|\varpi), & \mathbf{x} \in \text{matrix} \\ 0, & \mathbf{x} \notin \text{matrix} \end{cases} \tag{4}$$

The ensemble average of $H(\mathbf{x}|\varpi)$ over all possible realizations in which $\mathbf{x}$ is in the matrix can be expressed as (cf. Ju and Lee (2000) and Tohgo and Weng (1994))

$$\langle H\rangle_m(\mathbf{x}) = H^0 + \int_{\varpi_1}\{H(\mathbf{x}|\varpi_1) - H^0\}P(\varpi_1)d\varpi_1 + \int_{\varpi_2}\{H(\mathbf{x}|\varpi_2) - H^0\}P(\varpi_2)d\varpi_2 + \cdots \tag{5}$$

where $\langle\cdot\rangle$ signifies the ensemble average operator, $H^0 = \boldsymbol{\sigma}^0 : \mathbf{I}_d : \boldsymbol{\sigma}^0$ is the square of the far-field stress norm in the matrix, and $P(\varpi_q)$ denotes the probability density function for finding the q-phase $(q = 1, 2)$ configuration ϖ_q (fibers or voids) in the (random) composite (Ju and Lee, 2000).

2.2. The exterior-point Eshelby's tensor for a circular inclusion in a finite domain

The perturbed stress for any matrix point $\mathbf{x}$ due to a typical isolated q-phase inhomogeneity centered at $\mathbf{x}_q^{(1)}$ takes the form (cf. Ju and Chen (1994), Ju and Lee (2000))

$$\boldsymbol{\sigma}'(\mathbf{x}|\mathbf{x}_q^{(1)}) = \left[\mathbf{C}_0 \cdot \overline{\mathbf{G}}^F\left(\mathbf{x} - \mathbf{x}_q^{(1)}\right)\right] : \boldsymbol{\epsilon}_q^{*0} \tag{6}$$

where $\boldsymbol{\epsilon}_q^{*0}$ is the solution of the (elastic) eigenstrain $\boldsymbol{\epsilon}_q^*$ for the single inclusion problem of the q-phase and is given by

$$\boldsymbol{\epsilon}_q^{*0} = -(\mathbf{A}_q + \mathbf{S}^F)^{-1} : \boldsymbol{\epsilon}^0, \quad q = 1, 2 \tag{7}$$

in which the interior-point Eshelby's tensor for a circular inclusion $\mathbf{S}^F$ was previously given in Eqs. (5)–(7) of Kim and Lee (2009), and $\mathbf{A}_q$ is defined as $\mathbf{A}_q = [\mathbf{C}_q - \mathbf{C}_0]^{-1} \cdot \mathbf{C}_0$. In addition, the exterior-point Eshelby's tensor $\overline{\mathbf{G}}^F(\mathbf{x} - \mathbf{x}_q^{(1)})$ for a circular inclusion with the radius r_0 embedded at the center of a finite, circular RVE with the radius R was explicitly derived by Li et al. (2005) and Wang et al. (2005) by solving a pair of Fredholm type integral equations.

The exterior-point Eshelby's tensor for a circular inclusion in the finite RVE subjected to the Dirichlet (displacement) boundary condition can be written as (Li et al., 2005)

$$\begin{aligned}\overline{G}^F_{ijkl}(\mathbf{x}-\mathbf{x}^{(1)}_q) = \frac{\rho_0^2}{8(1-\nu)}\Bigg\{&\left[9\rho_0^2\left(\frac{1}{t^4}\right)-2(1+2\nu)\left(\frac{1}{t^2}\right)\right.\\&\left.+(1-4\nu)+\frac{3(\rho_0^2-1)}{4\nu-3}-\frac{12\nu(\rho_0^2-1)}{4\nu-3}(t^2)\right]\delta_{ij}\delta_{kl}\\&+\left[-3\rho_0^2\left(\frac{1}{t^4}\right)+2\left(\frac{1}{t^2}\right)-(3-4\nu)-\frac{3(\rho_0^2-1)}{4\nu-3}\right.\\&\left.+\frac{6(\rho_0^2-1)}{4\nu-3}(t^2)\right](\delta_{ik}\delta_{jl}+\delta_{il}\delta_{jk})+\left[-12\rho_0^2\left(\frac{1}{t^4}\right)\right.\\&\left.+4(1+2\nu)\left(\frac{1}{t^2}\right)-\frac{12(1-2\nu)(\rho_0^2-1)}{4\nu-3}(t^2)\right]\delta_{ij}n_kn_l\\&+\left[-12\rho_0^2\left(\frac{1}{t^4}\right)+4\left(\frac{1}{t^2}\right)\right]\delta_{kl}n_in_j\\&+\left[24\rho_0^2\left(\frac{1}{t^4}\right)-16\left(\frac{1}{t^2}\right)\right]n_in_jn_kn_l\Bigg\}\end{aligned}\tag{8}$$

where ν is the Poisson's ratio of the matrix, $\rho_0 = r_0/R$, $\rho = r_0/|\mathbf{x}|$, $t = \rho_0/\rho$, and $n_i(\mathbf{x}) = x_i/|\mathbf{x}|$ $(i = 1,2)$ are the components of the unit vector in the direction of the position vector $\mathbf{x}$ (Li et al., 2005; Wang et al., 2005). In case of the Neumann (traction) boundary condition, the exterior-point Eshelby's tensor can be derived as (Wang et al., 2005)

$$\begin{aligned}\overline{G}^F_{ijkl}\left(\mathbf{x}-\mathbf{x}^{(1)}_q\right) = \frac{\rho_0^2}{8(1-\nu)}\Bigg\{&\left[9\rho_0^2\left(\frac{1}{t^4}\right)-2(1+2\nu)\left(\frac{1}{t^2}\right)-2(1+2\nu)\right.\\&\left.+3\rho_0^2-12\nu(\rho_0^2-1)(t^2)\right]\delta_{ij}\delta_{kl}+\left[-3\rho_0^2\left(\frac{1}{t^4}\right)\right.\\&\left.+2\left(\frac{1}{t^2}\right)+(4-3\rho_0^2)+6(\rho_0^2-1)(t^2)\right](\delta_{ik}\delta_{jl}+\delta_{il}\delta_{jk})\\&+\left[-12\rho_0^2\left(\frac{1}{t^4}\right)+4(1+2\nu)\left(\frac{1}{t^2}\right)\right.\\&\left.-12(1-2\nu)(\rho_0^2-1)(t^2)\right]\delta_{ij}n_kn_l+\left[-12\rho_0^2\left(\frac{1}{t^4}\right)\right.\\&\left.+4\left(\frac{1}{t^2}\right)\right]\delta_{kl}n_in_j+\left[24\rho_0^2\left(\frac{1}{t^4}\right)-16\left(\frac{1}{t^2}\right)\right]n_in_jn_kn_l\Bigg\}\end{aligned}\tag{9}$$

2.3. A first-order formulation of effective elastoplastic behavior of fiber-reinforced ductile composites

The total stress at any point $\mathbf{x}$ in the matrix can be the superposition of the far-field stress $\boldsymbol{\sigma}^0$ and the perturbed stress $\boldsymbol{\sigma}'$ due to the presence of the fibers and voids (Ju and Lee, 2000).

$$\boldsymbol{\sigma}(\mathbf{x}) = \boldsymbol{\sigma}^0 + \boldsymbol{\sigma}'(\mathbf{x})\tag{10}$$

in which $\boldsymbol{\sigma}^0$ and $\boldsymbol{\sigma}'$ are defined as

$$\boldsymbol{\sigma}^0 \equiv \mathbf{C}_0 : \boldsymbol{\epsilon}^0\tag{11}$$

$$\boldsymbol{\sigma}' \equiv \mathbf{C}_0 : \int_A \overline{\mathbf{G}}^F(\mathbf{x}-\mathbf{x}') : \boldsymbol{\epsilon}^*_1(\mathbf{x}')d\mathbf{x}' + \mathbf{C}_0 : \int_A \overline{\mathbf{G}}^F(\mathbf{x}-\mathbf{x}') : \boldsymbol{\epsilon}^*_2(\mathbf{x}')d\mathbf{x}'\tag{12}$$

where $\boldsymbol{\epsilon}^0$ is the elastic strain field induced by the far-field loading, $\boldsymbol{\epsilon}^*_q(\mathbf{x}')$ denotes the elastic eigenstrain in the q-phase $(q = 1,2)$, and $\mathbf{x}'$ resides in either a fiber or a void, and A is the area of RVE.

Following Ju and Lee (2000), Ju and Zhang (2001), and Lee and Pyo (2008), the ensemble-average stress norm for any point $\mathbf{x}$ given in Eq. (5) can be evaluated by collecting and summing up all the current stress norm perturbation produced by any typical fiber or void centered at $\mathbf{x}^{(1)}_q$ $(q = 1,2)$ in the fiber or void domains and averaging over all possible locations of $\mathbf{x}^{(1)}_q$ as

$$\begin{aligned}\langle H\rangle_m(\mathbf{x}) \cong H^o &+ \int_{|\mathbf{x}-\mathbf{x}^{(1)}_1|}^{=r_0|\mathbf{x}-\mathbf{x}^{(1)}_1|=R}\left\{H\left(\mathbf{x}|\mathbf{x}^{(1)}_1\right)-H^o\right\}P(\mathbf{x}^{(1)}_1)\,d\mathbf{x}^{(1)}_1\\&+\int_{|\mathbf{x}-\mathbf{x}^{(1)}_2|}^{=r_0|\mathbf{x}-\mathbf{x}^{(1)}_2|=R}\left\{H\left(\mathbf{x}|\mathbf{x}^{(1)}_2\right)-H^o\right\}P\left(\mathbf{x}^{(1)}_2\right)\,d\mathbf{x}^{(1)}_2+\cdots\end{aligned}\tag{13}$$

where the probability density function for finding a fiber or a void centered at $\mathbf{x}^{(1)}_q$ is assumed to take the form $P\left(\mathbf{x}^{(1)}_q\right) = N_q/A$, in which $N_q(=\phi_q/\rho_0^2)$ is the total numbers of fibers or voids dispersed in a representative area A. Eq. (13) can be further recast into a more simplified form (cf. Ju and Zhang, 2001):

$$\begin{aligned}\langle H\rangle_m(\mathbf{x}) \cong H^0 &+ \frac{N_1}{A}\int_0^{2\pi}\int_{r_0}^R r_1\{H(\mathbf{r}_1)-H^0\}dr_1d\theta\\&+\frac{N_2}{A}\int_0^{2\pi}\int_{r_0}^R r_2\{H(\mathbf{r}_2)-H^0\}dr_2d\theta\end{aligned}\tag{14}$$

where $\mathbf{r}_q = \mathbf{x}-\mathbf{x}_q$ and $r_q = \|\mathbf{r}_q\|$.

During the ensemble average evaluation of the surface integrals, the following three different integral identity groups are discovered (cf. Ju and Lee, 2001).

(i) When the integrand $[H(\mathbf{r}_q)-H^0]$ does not have n_i, we have

$$\begin{aligned}&\int_{r_0}^R\int_0^{2\pi} r\,dr\,d\theta = \pi R^2(1-\alpha)\\&\int_{r_0}^R\int_0^{2\pi}\frac{r}{t^2}dr\,d\theta = \int_{r_0}^R\int_0^{2\pi}\frac{R^2}{r}dr\,d\theta = -\pi R^2\ln\alpha\\&\int_{r_0}^R\int_0^{2\pi}\frac{r}{t^4}dr\,d\theta = \int_{r_0}^R\int_0^{2\pi}\frac{R^4}{r^3}dr\,d\theta = \pi R^2\left(\frac{1}{\alpha}-1\right)\\&\int_{r_0}^R\int_0^{2\pi}\frac{r}{t^6}dr\,d\theta = \int_{r_0}^R\int_0^{2\pi}\frac{R^6}{r^5}dr\,d\theta = \frac{\pi R^2}{2}\left(\frac{1}{\alpha^2}-1\right)\\&\int_{r_0}^R\int_0^{2\pi}\frac{r}{t^8}dr\,d\theta = \int_{r_0}^R\int_0^{2\pi}\frac{R^8}{r^7}dr\,d\theta = \frac{\pi R^2}{3}\left(\frac{1}{\alpha^3}-1\right)\\&\int_{r_0}^R\int_0^{2\pi} rt^2dr\,d\theta = \int_{r_0}^R\int_0^{2\pi}\frac{r^3}{R^2}dr\,d\theta = \frac{\pi R^2}{2}(1-\alpha^2)\\&\int_{r_0}^R\int_0^{2\pi} rt^4dr\,d\theta = \int_{r_0}^R\int_0^{2\pi}\frac{r^5}{R^4}dr\,d\theta = \frac{\pi R^2}{3}(1-\alpha^3)\end{aligned}\tag{15}$$

in which $\alpha = \rho_0^2$.

(ii) When the integrand $[H(\mathbf{r}_q)-H^0]$ has n_in_j, we have

$$\begin{aligned}&\int_{r_0}^R\int_0^{2\pi} rn_in_j\,dr\,d\theta = \frac{\pi R^2}{2}(1-\alpha)\delta_{ij}\\&\int_{r_0}^R\int_0^{2\pi}\frac{r}{t^2}n_in_j\,dr\,d\theta = \int_{r_0}^R\int_0^{2\pi}\frac{R^2}{r}n_in_j\,dr\,d\theta = -\frac{\pi R^2}{2}(\ln\alpha)\delta_{ij}\\&\int_{r_0}^R\int_0^{2\pi}\frac{r}{t^4}n_in_j\,dr\,d\theta = \int_{r_0}^R\int_0^{2\pi}\frac{R^4}{r^3}n_in_j\,dr\,d\theta = \frac{\pi R^2}{2}\left(\frac{1}{\alpha}-1\right)\delta_{ij}\\&\int_{r_0}^R\int_0^{2\pi}\frac{r}{t^6}n_in_j\,dr\,d\theta = \int_{r_0}^R\int_0^{2\pi}\frac{R^6}{r^5}n_in_j\,dr\,d\theta = \frac{\pi R^2}{4}\left(\frac{1}{\alpha^2}-1\right)\delta_{ij}\\&\int_{r_0}^R\int_0^{2\pi}\frac{r}{t^8}n_in_j\,dr\,d\theta = \int_{r_0}^R\int_0^{2\pi}\frac{R^8}{r^7}n_in_j\,dr\,d\theta = \frac{\pi R^2}{6}\left(\frac{1}{\alpha^3}-1\right)\delta_{ij}\\&\int_{r_0}^R\int_0^{2\pi} rt^2n_in_j\,dr\,d\theta = \int_{r_0}^R\int_0^{2\pi}\frac{r^3}{R^2}n_in_j\,dr\,d\theta = \frac{\pi R^2}{4}(1-\alpha^2)\delta_{ij}\\&\int_{r_0}^R\int_0^{2\pi} rt^4n_in_j\,dr\,d\theta = \int_{r_0}^R\int_0^{2\pi}\frac{r^5}{R^4}n_in_j\,dr\,d\theta = \frac{\pi R^2}{6}(1-\alpha^3)\delta_{ij}\end{aligned}\tag{16}$$

(iii) When the integrand $[H(\mathbf{r}_q) - H^0]$ has $n_i n_j n_k n_l$, we have

$$\int_{r_0}^{R}\int_0^{2\pi} r n_i n_j n_k n_l dr d\theta = \frac{\pi R^2}{8}(1-\alpha)(\delta_{ij}\delta_{kl}+\delta_{ik}\delta_{jl}+\delta_{il}\delta_{jk})$$

$$\int_{r_0}^{R}\int_0^{2\pi} \frac{r}{t^2} n_i n_j n_k n_l dr d\theta = \int_{r_0}^{R}\int_0^{2\pi} \frac{R^2}{r} n_i n_j n_k n_l dr d\theta = -\frac{\pi R^2}{8}(\ln\alpha)(\delta_{ij}\delta_{kl}+\delta_{ik}\delta_{jl}+\delta_{il}\delta_{jk})$$

$$\int_{r_0}^{R}\int_0^{2\pi} \frac{r}{t^4} n_i n_j n_k n_l dr d\theta = \int_{r_0}^{R}\int_0^{2\pi} \frac{R^4}{r^3} n_i n_j n_k n_l dr d\theta = \frac{\pi R^2}{8}\left(\frac{1}{\alpha}-1\right)(\delta_{ij}\delta_{kl}+\delta_{ik}\delta_{jl}+\delta_{il}\delta_{jk})$$

$$\int_{r_0}^{R}\int_0^{2\pi} \frac{r}{t^6} n_i n_j n_k n_l dr d\theta = \int_{r_0}^{R}\int_0^{2\pi} \frac{R^6}{r^5} n_i n_j n_k n_l dr d\theta = \frac{\pi R^2}{16}\left(\frac{1}{\alpha^2}-1\right)(\delta_{ij}\delta_{kl}+\delta_{ik}\delta_{jl}+\delta_{il}\delta_{jk})$$

$$\int_{r_0}^{R}\int_0^{2\pi} \frac{r}{t^8} n_i n_j n_k n_l dr d\theta = \int_{r_0}^{R}\int_0^{2\pi} \frac{R^8}{r^7} n_i n_j n_k n_l dr d\theta = \frac{\pi R^2}{24}\left(\frac{1}{\alpha^3}-1\right)(\delta_{ij}\delta_{kl}+\delta_{ik}\delta_{jl}+\delta_{il}\delta_{jk}) \quad (17)$$

$$\int_{r_0}^{R}\int_0^{2\pi} r t^2 n_i n_j n_k n_l dr d\theta = \int_{r_0}^{R}\int_0^{2\pi} \frac{r^3}{R^2} n_i n_j n_k n_l dr d\theta = \frac{\pi R^2}{16}(1-\alpha^2)(\delta_{ij}\delta_{kl}+\delta_{ik}\delta_{jl}+\delta_{il}\delta_{jk})$$

$$\int_{r_0}^{R}\int_0^{2\pi} r t^4 n_i n_j n_k n_l dr d\theta = \int_{r_0}^{R}\int_0^{2\pi} \frac{r^5}{R^4} n_i n_j n_k n_l dr d\theta = \frac{\pi R^2}{24}(1-\alpha^3)(\delta_{ij}\delta_{kl}+\delta_{ik}\delta_{jl}+\delta_{il}\delta_{jk})$$

By using the above three integral identity groups and the perturbed stress given in Eq. (14), the ensemble-averaged current stress norm at any point in the matrix can be derived as

$$\langle H\rangle_m(\mathbf{x}) = \boldsymbol{\sigma}^0 : \mathbf{T} : \boldsymbol{\sigma}^0 \quad (18)$$

where the components of the positive definite fourth-rank tensor $\mathbf{T}$ read

$$T_{ijkl} = T_1\delta_{ij}\delta_{kl} + T_2(\delta_{ik}\delta_{jl}+\delta_{il}\delta_{jk}) \quad (19)$$

with

$$T_1 = -\frac{1}{2} + F_1^{[1]} + F_1^{[2]}, \quad T_2 = \frac{1}{2} + F_2^{[1]} + F_2^{[2]} \quad (20)$$

where the parameters $F_1^{[q]}$ and $F_2^{[q]}$ $(q = 1, 2)$ are given in Appendix A.

Following Ju and Lee (2001) and Lee and Simunovic (2001), the relation between the far-field stress $\boldsymbol{\sigma}^o$ and the macroscopic stress $\bar{\boldsymbol{\sigma}}$ can be expressed as

$$\boldsymbol{\sigma}^o = \mathbf{P} : \bar{\boldsymbol{\sigma}} \quad (21)$$

where the components of the fourth-rank tensor $\mathbf{P}$ are

$$P_{ijkl} = P_1\delta_{ij}\delta_{kl} + P_2(\delta_{ik}\delta_{jl}+\delta_{il}\delta_{jk}) \quad (22)$$

with

$$P_1 = -\frac{\Gamma_1}{4\Gamma_2(\Gamma_1+\Gamma_2)}, \quad P_2 = \frac{1}{4\Gamma_2} \quad (23)$$

and the coefficients Γ_1 and Γ_2 read:

$$\Gamma_1 = 2\phi_1\left[-S_1\omega_1^{[1]} - S_1\omega_2^{[1]} + \omega_1^{[1]}\left(\frac{1}{2}-S_2\right)\right] + 2\phi_2\left[-S_1\omega_1^{[2]} - S_1\omega_2^{[2]} + \omega_1^{[2]}\left(\frac{1}{2}-S_2\right)\right] \quad (24)$$

$$\Gamma_2 = \frac{1}{2} + 2\phi_1\omega_2^{[1]}\left(\frac{1}{2}-2S_2\right) + 2\phi_2\omega_2^{[2]}\left(\frac{1}{2}-2S_2\right) \quad (25)$$

The ensemble-averaged current stress norm in a matrix can be recast by combining Eqs. (19) and (22) as

$$\langle H\rangle_m(\mathbf{x}) = \bar{\boldsymbol{\sigma}} : \overline{\mathbf{T}} : \bar{\boldsymbol{\sigma}} \quad (26)$$

where the positive definite fourth-rank tensor $\overline{\mathbf{T}}$ is defined as

$$\overline{\mathbf{T}} \equiv \mathbf{P}^{\mathbf{T}} \cdot \mathbf{T} \cdot \mathbf{P} \quad (27)$$

and can be derived as

$$\overline{T}_{ijkl} = \overline{T}_1\delta_{ij}\delta_{kl} + \overline{T}_2(\delta_{ik}\delta_{jl}+\delta_{il}\delta_{jk}) \quad (28)$$

in which

$$\overline{T}_1 = 4[(P_1+P_2)(P_1T_1+P_1T_2+P_2T_1)+P_2T_2P_1], \quad \overline{T}_2 = 4P_2T_2P_2 \quad (29)$$

According to Ju and Lee (2000), Lee and Simunovic (2001), and Lee and Pyo (2008), the ensemble-averaged current stress norm for any point $\mathbf{x}$ in the three-phase composite can be defined as

$$\sqrt{\langle H\rangle(\mathbf{x})} = (1-\phi_1)\sqrt{\bar{\boldsymbol{\sigma}} : \overline{\mathbf{T}} : \bar{\boldsymbol{\sigma}}} \quad (30)$$

where ϕ_1 is the volume fraction of current perfectly bonded fibers. Accordingly, the effective yield function for the three-phase composite given in Eq. (3) becomes

$$\overline{F} = (1-\phi_1)\sqrt{\bar{\boldsymbol{\sigma}} : \overline{\mathbf{T}} : \bar{\boldsymbol{\sigma}}} - K(\bar{e}^p) \quad (31)$$

For simplicity, the following simple power-law type isotropic hardening function is adopted here.

$$K(\bar{e}^p) = \sqrt{\frac{2}{3}}\{\sigma_y + h(\bar{e}^p)^q\} \quad (32)$$

where σ_y denotes the initial yield stress, and h and q signify the linear and exponential isotropic hardening parameters, respectively (see also Ju and Lee (2000)). The effective ensemble-averaged plastic strain rate $\dot{\bar{e}}^p$ and the effective equivalent plastic strain rate $\dot{\bar{e}}^p$ required for obtaining the ensemble-averaged current stress norm were given in Eqs. (61) and (62) of Ju and Zhang (2001), respectively.

2.4. Elastoplastic stress–strain relation under uniaxial tension

The elastoplastic stress–strain relation under uniaxial tensile loading of the proposed micromechanical framework is formulated in this subsection. The applied macroscopic stress $\bar{\boldsymbol{\sigma}}$ under the plane-strain condition can be written as

$$\bar{\sigma}_{11} > 0, \quad \bar{\sigma}_{33} = \nu_A^*\bar{\sigma}_{11}, \quad \text{all other } \bar{\sigma}_{ij} = 0 \quad (33)$$

Accordingly, the effective yield function in Eq. (31) can be rephrased for the uniaxial loading case as (Ju and Zhang, 2001; Ju et al., 2006)

$$\overline{F}(\bar{\sigma}_{11}, \bar{e}^p) = (1-\phi_1)\sqrt{(\overline{T}_1+2\overline{T}_2)}\bar{\sigma}_{11} - \sqrt{\frac{2}{3}}\{\sigma_y + h(\bar{e}^p)^q\} \quad (34)$$

Following Ju and Zhang (2001) and Ju et al. (2006), the overall macroscopic stress–strain relation for the monotonic plane-strain uniaxial loading can be obtained as

$$\bar{\epsilon} = \begin{bmatrix} E_A^* - E_T^*\nu_A^{*2} & 0 \\ 0 & -E_A^*\nu_T^* - E_T^*\nu_A^{*2} \end{bmatrix}\frac{\bar{\sigma}_{11}}{E_T^*E_A^*} + (1-\phi_1)\frac{\lambda}{\sqrt{(\overline{T}_1+2\overline{T}_2)}}\begin{bmatrix} \overline{T}_1+2\overline{T}_2 & 0 \\ 0 & \overline{T}_1 \end{bmatrix} \quad (35)$$

where λ is the positive parameter and was obtained previously by the plastic consistency condition $\overline{F} = 0$ (see, e.g., Ju and Zhang,

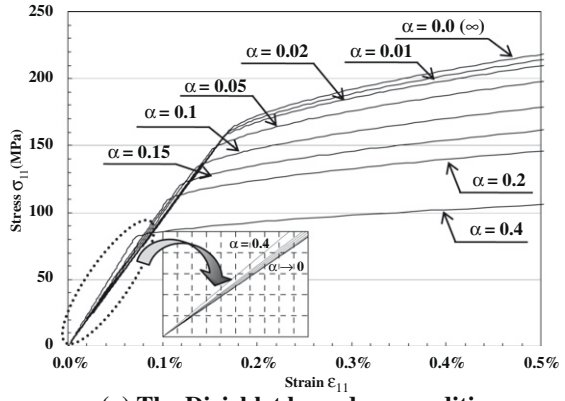

(a) The Dirichlet boundary condition

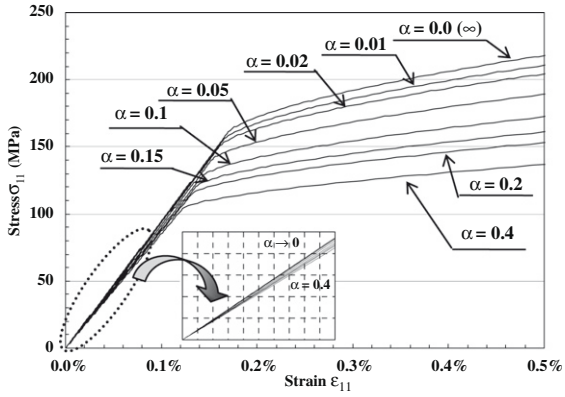

(b) The Neumann boundary condition

Fig. 2. The predicted stress–strain curves of circular fiber-reinforced composites with various α values.

2001; Ju et al., 2006). In addition, the effective transverse and axial Young's modulus E_T^* and E_A^*, and effective transverse and axial Poisson's ratios v_T^* and v_A^* of the composite can be found from Eqs. 31, 32, 33, 35a of Hashin (1972) and Eqs. (16)–(20) of Ju and Zhang (2001).

3. Numerical simulations

The proposed elastoplastic model is exercised to predict the elastoplastic behavior of circular fiber-reinforced composites under uniaxial tension in the transverse direction. The elastoplastic behavior of 2024 aluminum alloy composites reinforced with unidirectionally aligned boron fibers (34% in fiber volume fraction) quoted by Ju and Zhang (2001) is predicted using the proposed model. The material properties of the matrix and fibers reported by Ju and Zhang (2001) are used: $E_m = 55.85$ GPa, $v_m = 0.32$, and $E_f = 379.23$ GPa, $v_f = 0.20$, where the subscripts m and f denote the matrix and fibers, respectively. The same plastic parameters as used in Ju and Zhang (2001) are also employed: $\sigma_y = 79.29$ MPa, $h = 827.4$ MPa and $q = 0.6$.

Various values of the parameter α, which is related to the ratio of the volume of the fiber to volume of the RVE, are considered in the simulation to examine the influence of the parameter α on the elastoplastic stress–strain behavior of the composites. The predicted stress–strain curves of the composites with various α values are shown in Fig. 2. It is seen from the figure that the predicted stress–strain curves converge to that obtained from the infinite RVE model as the parameter α continues to decrease. The effect of the parameter α on the plastic behavior beyond the yielding point is shown to be more influential than that on the elastic behavior.

A parametric analysis is conducted to examine the influence of the Weibull parameter S_0 on the overall elastoplastic damage behavior of circular fiber-reinforced composites. Fig. 3 exhibits a flowchart describing step-by-step algorithms used for the prediction of the elastoplastic behavior of circular fiber-reinforced composites considering evolutionary damage. The symbol I in the flowchart is used to denote the iteration number of stress increment until the final stage and the symbol N signifies the maximum iteration number (e.g. $N = 100$). The elastoplastic behavior of SiC/Ti–6Al–4V composites (fiber volume fraction of 32%) with various S_0 values is predicted. The material properties and plastic parameters are adopted in accordance with Ju and Ko (2008) as: $E_m = 113.7$ GPa, $v_m = 0.3$, $E_f = 414.0$ GPa, $v_f = 0.3$; $\sigma_y = 500.0$ MPa, $h = 700.0$ MPa, $q = 0.1$. Two different S_0 values ($S_0 = 1.09 \times \sigma_y$ and $S_0 = 0.59 \times \sigma_y$) with two different boundary conditions (the Dirichlet and the Neumann boundary conditions) are used in the parametric analysis. Another Weibull parameter M is fixed as follows: $M = 3.0$.

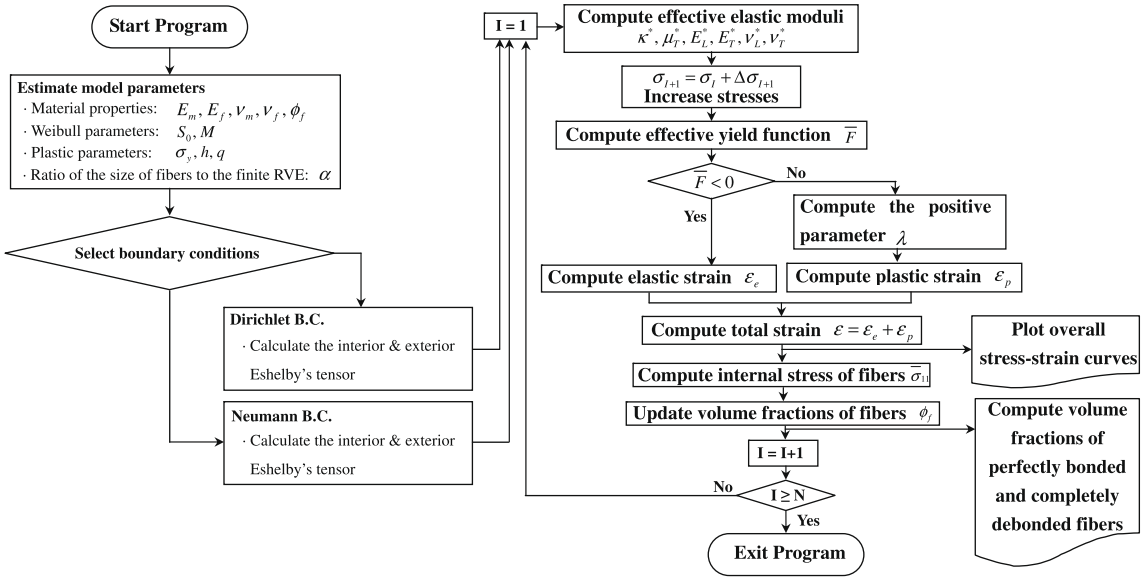

Fig. 3. The flowchart describing step-by-step algorithms used for the present numerical simulations.

The present predicted elastoplastic stress–strain responses of the composites with two different S_0 values and the two different boundary conditions under uniaxial tension are plotted in Fig. 4. Portions of the stress–strain curves experiencing severe interfacial damage together with the corresponding evolution of volume fractions of perfectly bonded fibers and completely debonded fibers are exhibited in Fig. 5. Typical three-stage elastoplastic stress–strain responses, which have also been observed and reported by other researchers (e.g., Majumdar and Newaz (1992), Nimmer et al. (1991) and Ju and Ko (2008)), are observed in Fig. 4. The linear portion of the curves in Fig. 4 is the first stage response featuring that fibers are perfectly bonded and the composites behaves yet elastically, some fibers begin to debond as shown in Parts A–D of Fig. 5 as strain continues to increase (the second stage), and the composites reach elastoplastic stage (the final stage) after the yielding stress. Smooth and gradual transitions from perfectly bonded fibers to completely debonded fibers occur with the Dirichlet boundary condition as shown in Fig. 5(b) and (d), whereas slight sharp progressions are observed in the evolutions of perfectly bonded fibers and completely debonded fibers with the Neumann boundary condition as shown in Fig. 5(f) and (h). It is also obvious from the Figs. 4 and 5 that lower Weibull parameter S_0 leads to lower elastoplastic stress–strain responses.

4. Experimental comparisons

Comparisons between the present predictions and experiments on SiC/Ti–6Al–4V composites conducted by Nimmer et al. (1991) and Sun et al. (1990) are made to further assess the predictive capability of the proposed model. A similar comparison between predictions (Ju et al., 2006) and the experiment (Nimmer et al., 1991) on the same composites was also reported by Ju et al. (2006). The material properties of the composites used in the simulations are (Sun et al., 1990; Nimmer et al., 1991; Li and Wisnom, 1996): $E_m = 110\,\text{GPa}, \nu_m = 0.33, E_f = 414\,\text{GPa}, \nu_f = 0.19; \sigma_y = 970\,\text{MPa}$. The volume fraction of fibers of the composites used in Sun et al. (1990)'s experiment was 40%, while the composites with two different fiber volume fractions 32% and 34% were used in Nimmer et al. (1991)'s experiments. The α value for the composites used in Sun et al. (1990)'s experiment is calculated to be $\alpha = 0.41$, whereas the α values for the composites with two different fiber volume fractions 32% and 34% used in Nimmer et al. (1991)'s experiments are calculated to be 0.33 and 0.35, respectively.

In accordance with the boundary condition of the specimens used in their experiments, the Dirichlet boundary condition is used in the present predictions. Since the model parameters S_0, M, h, and q were not reported in Sun et al. (1990) and Nimmer et al. (1991), they are estimated by fitting an experimentally obtained stress–strain curve (Sun et al., 1990) with the present prediction. The model parameters are estimated to be $S_0 = 0.436 \times \sigma_y, M = 1.5; h = 1.8$ GPa, $q = 0.07$. Fig. 6(a) shows the comparison between the present prediction based on the above material properties and parameters and the experimental data (Sun et al., 1990) on the overall elastoplastic stress–strain response of the composites. Overall, the present prediction and the experimental data match well. The predicted damage evolution curves corresponding to the Fig. 6(a) are shown in Fig. 6(b).

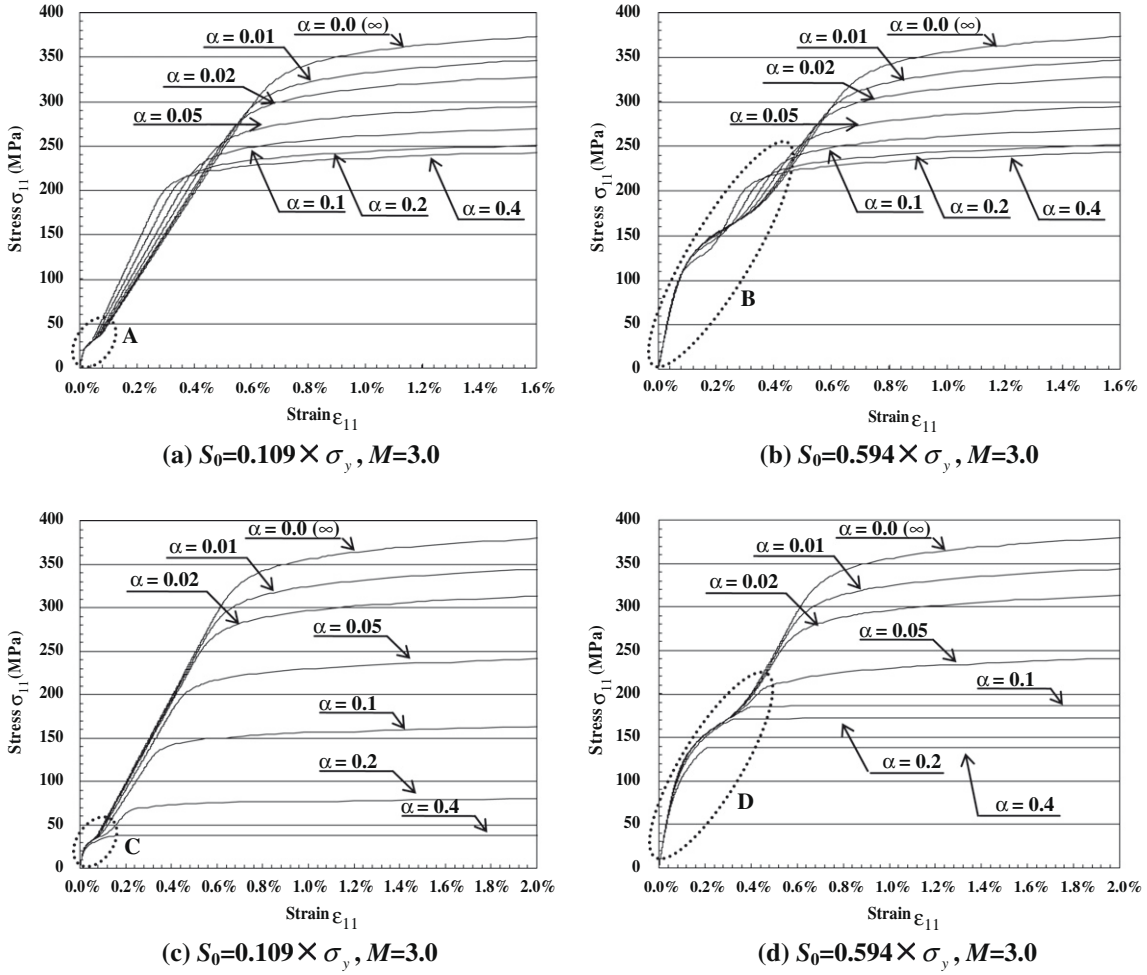

Fig. 4. The predicted stress–strain curves of SiC/Ti–6Al–4V composites with the Dirichlet boundary condition [(a) and (b)] and the Neumann boundary condition [(c) and (d)].

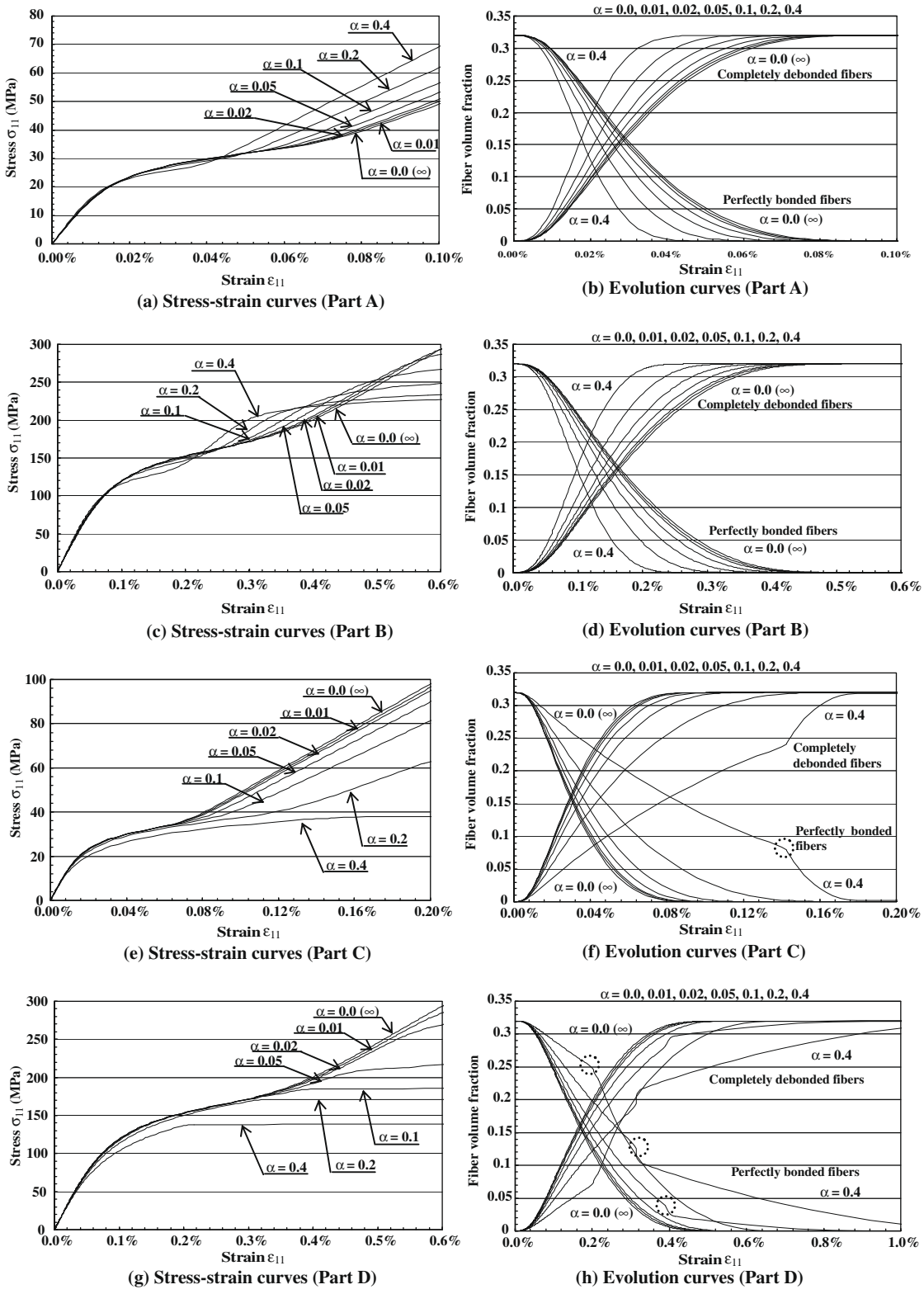

Fig. 5. Portions of the stress–strain curves in Fig. 4 experiencing severe damage, and the corresponding the damage evolutions curves.

The proposed elastoplastic model is further exercised to predict the behavior of the composites reported in Nimmer et al. (1991). Fig. 6(c) and (e) show the comparisons of stress–strain curves between the present predictions and the experimental data on the composites with fiber volume fractions of 32% and 34%, respectively (Nimmer et al., 1991). The evolution of volume fractions of perfectly bonded fibers and completely debonded fibers corresponding to Fig. 6(c) and (e) are exhibited in Fig. 6(d) and (f), respectively. Good agreements between the present predictions and the experiments (Nimmer et al., 1991) are also observed in Fig. 6(c) and (e).

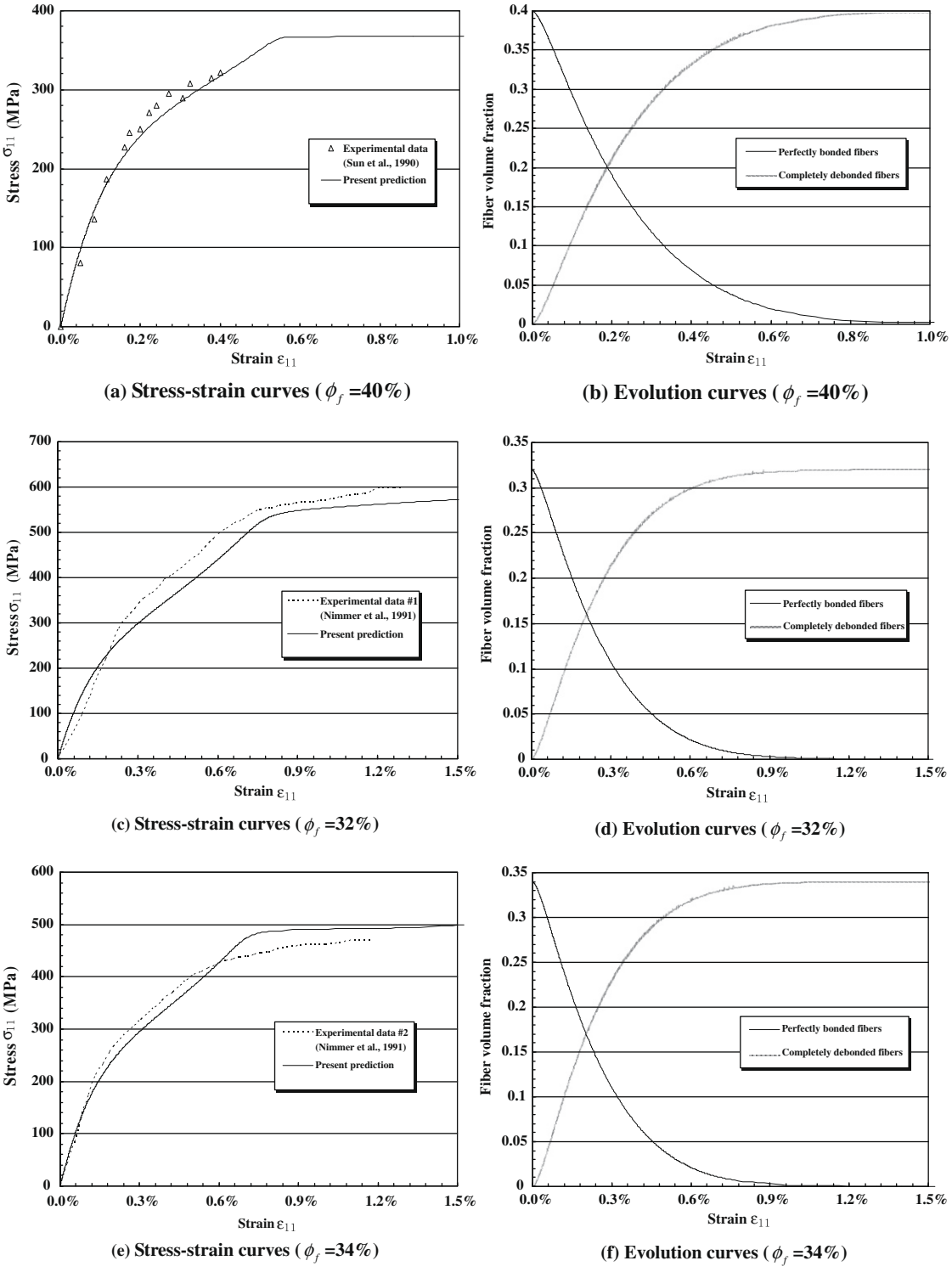

Fig. 6. The comparison of stress–strain curves between the present prediction and the experimental data [34, 38] and the evolution of perfectly bonded and completely debonded fibers corresponding the stress–strain curves.

5. Concluding remarks

A micromechanical elastoplastic damage model considering a finite RVE has been presented to predict the overall elastoplastic damage behavior of circular fiber-reinforced ductile composites. A micromechanical framework to predict the effective elastoplastic damage responses of ductile composites is derived based on the exterior-point Eshelby's tensor for circular inclusions and the ensemble-averaged effective yield criterion. A series of numerical simulations and experimental comparisons are conducted to illustrate and assess the predictive capability of the proposed model. The findings of this numerical study can be summarized as: (1) the present predicted stress–strain curves converge to that obtained from the infinite RVE model as the parameter α continues to decrease. (2) The effect of the parameter α on the plastic behavior beyond the yielding point is shown to be more influential than

that on the elastic behavior. (3) Typical three-stage elastoplastic stress–strain responses are observed in the predicted stress–strain curves. (4) Smooth and gradual transitions from perfectly bonded fibers to completely debonded fibers occur with the Dirichlet boundary condition, whereas slight sharp progressions are observed in the evolutions of perfectly bonded fibers and completely debonded fibers with the Neumann boundary condition. (5) Lower Weibull parameter S_0 leads to lower elastoplastic stress–strain responses. (6) Good agreements between the present predictions and experimental data verify the predictive capability of the model.

This study has demonstrated the capability of the proposed micromechanical framework for predicting the elastoplastic damage behavior of circular fiber-reinforced composites. In particular, the proposed micromechanical elastoplastic model is suitable for predicting the behavior of fiber-reinforced ductile composites having moderately large circular fibers. However, a unified experimental and numerical study needs to be carried out for the calibration of the model parameters of the proposed model.

Acknowledgments

This research was sponsored by the IT R&D program of MKE/IITA (2008-F-044-01, Development of new IT convergence technology for smart building to improve the environment of electromagnetic waves, sound and building) and the Smart Infra-Structure Technology Center (SISTeC) program of KOSEF (R11-2002-101-02003 (2008)).

Appendix A. Parameters $F_1^{[q]}$ and $F_2^{[q]}$ $(q = 1, 2)$ in Eq. (20)

The parameters $F_1^{[q]}$ and $F_2^{[q]}$ $(q = 1, 2)$ in Eq. (20) take the form

$$\begin{aligned} F_1^{[q]} = \frac{\phi_q \rho_0^4}{8(1-\nu)^2}\Big[& (4\xi^{[q]2} + 4\xi^{[q]}\eta^{[q]} + 7\eta^{[q]2})\Lambda_1^2 \subset \frac{r}{t^8} \supset \\ & - 2(\xi^{[q]2} + 2\xi^{[q]}\eta^{[q]} + 4\eta^{[q]2})\Lambda_1\Lambda_2 \subset \frac{r}{t^6} \supset \\ & + \Big\{(7\xi^{[q]2} + 6\xi^{[q]}\eta^{[q]} + 6\eta^{[q]2})\Lambda_2^2 \\ & + 4(\xi^{[q]2} + \xi^{[q]}\eta^{[q]} + 2\eta^{[q]2})\Lambda_1\Lambda_3\Big\} \subset \frac{r}{t^4} \supset \\ & + 4(\xi^{[q]2} + \xi^{[q]}\eta^{[q]} + 2\eta^{[q]2})(\Lambda_1\Lambda_4 + \Lambda_2\Lambda_3) \subset \frac{r}{t^2} \supset \\ & + 4(\xi^{[q]2} + \xi^{[q]}\eta^{[q]} + 2\eta^{[q]2})\Lambda_2\Lambda_4 \subset r \supset \\ & - 2\eta^{[q]2}\Lambda_3\Lambda_4 \subset rt^2 \supset -\eta^{[q]2}\Lambda_4^2 \subset rt^4 \supset \\ & + \frac{\phi_q\eta^{[q]}\rho_0^2}{2(1-\nu)}[\Lambda_3 \subset r \supset + \Lambda_4 \subset rt^2 \supset \Big] \end{aligned} \tag{36}$$

$$\begin{aligned} F_2^{[q]} = \frac{\phi_q \eta^{[q]2}\rho_0^4}{8(1-\nu)^2}\Big[& \Lambda_1^2 \subset \frac{r}{t^8} \supset + 2\Lambda_1\Lambda_2 \subset \frac{r}{t^6} \supset + \Lambda_2^2 \subset \frac{r}{t^4} \supset \\ & + 2\Lambda_3\Lambda_4 \subset rt^2 \supset + \Lambda_4^2 \subset rt^4 \supset \Big] \\ & - \frac{\phi_q\eta^{[q]}\rho_0^2}{2(1-\nu)}[\Lambda_3 \subset r \supset + \Lambda_4 \subset rt^2 \supset] \end{aligned} \tag{37}$$

where ϕ_q is the volume fraction of q-phase, $\subset \cdot \supset$ denotes the integral intentity groups described in Eqs. (15)–(17) in which "$\cdot$" signifies the integrand of the integral intentity groups, and the parameters $\xi^{[q]}$ and $\eta^{[q]}$ are given by

$$\xi^{[q]} = -\frac{\lambda_0}{2\mu_0(\lambda_0+\mu_0)}\left(\omega_1^{[q]} + \omega_2^{[q]}\right) + \eta^{[q]}, \quad \eta^{[q]} = \frac{\omega_2^{[q]}}{2\mu_0} \tag{38}$$

with

$$\begin{aligned} \omega_1^{[1]} &= -\frac{\varrho_1}{4\varrho_2(\varrho_1+\varrho_2)}, \quad \omega_2^{[1]} = \frac{1}{4\varrho_2}, \\ \omega_1^{[2]} &= -\frac{S_1}{(2S_2-1)(2S_1+2S_2-1)}, \quad \omega_2^{[2]} = \frac{1}{2(2S_2-1)} \end{aligned} \tag{39}$$

and the coefficients ϱ_1 and ϱ_2 are

$$\begin{aligned} \varrho_1 &= S_1 + \frac{\lambda_0}{2(\mu_1-\mu_0)} - \frac{\lambda_0+\mu_0}{2(\lambda_1-\lambda_0+\mu_1-\mu_0)}, \\ \varrho_2 &= S_2 + \frac{\mu_0}{2(\mu_1-\mu_0)} \end{aligned} \tag{40}$$

where the components of the interior-point Eshelby's tensor S_1 and S_2 for a circular inclusion can be found in Li et al. (2005), Wang et al. (2005), and Kim and Lee (2009).

In addition, the parameters Λ_i $(i = 1, \ldots, 4)$ in Eqs. (36) and (37) in case of the Dirichlet (displacement) boundary condition read:

$$\begin{aligned} \Lambda_1 &= -6\mu_0\rho_0^2, \quad \Lambda_2 = 4\mu_0, \\ \Lambda_3 &= -2\mu_0\left[(3-4\nu_0) + \frac{3(\rho_0^2-1)}{4\nu_0-3}\right], \\ \Lambda_4 &= 12\nu_0\frac{\rho_0^2-1}{4\nu_0-3} \end{aligned} \tag{41}$$

In case of the Neumann (traction) boundary condition, the parameters are

$$\begin{aligned} \Lambda_1 &= -6\mu_0\rho_0^2, \quad \Lambda_2 = 4\mu_0, \\ \Lambda_3 &= 2\mu_0(4-3\rho_0^2), \quad \Lambda_4 = 12\nu_0(\rho_0^2-1) \end{aligned} \tag{42}$$

References

Bansal, N.P., Eldridge, J.I., 1999. Effects of fiber/matrix interface and its composition on mechanical properties of Hi-Nicalon/Celsian composites. NASA TM-1999.
Caporale, A., Luciano, R., Sacco, E., 2006. Micromechanical analysis of interfacial debonding in unidirectional fiber-reinforced composites. Comput. Struct. 84, 2200–2211.
Chiang, Y.C., 2001. On fiber debonding and matrix cracking in fiber-reinforced ceramics. Compos. Sci. Technol. 61, 1743–1756.
Eshelby, J.D., 1957. The determination of the elastic field of an ellipsoidal inclusion and related problems. P. Roy. Soc. Lon. A 241, 376–396.
Eshelby, J.D., 1959. The elastic field outside an ellipsoidal inclusion. P. Roy. Soc. Lon. A 252, 561–569.
Hashin, Z., 1972. Analysis of properties of fiber composites with anisotropic constituents. ASME J. Appl. Mech. 46, 543–550.
Hill, R., 1950. The Mathematical Theory of Plasticity. Clarendon, Oxford.
Huang, W.C., 1971. Plastic behavior of some composite materials. J. Compos. Mater. 5, 320–338.
Ju, J.W., Chen, T.M., 1994. Micromechanics and effective elastoplastic behavior of two-phase metal matrix composites. J. Eng. Mater. Technol.-T ASME 116, 310–318.
Ju, J.W., Ko, Y.F., Ruan, H.N., 2006. Effective elastoplastic damage mechanics for fiber reinforced composites with evolutionary complete fiber debonding. Int. J. Damage Mech. 15, 237–265.
Ju, J.W., Ko, Y.F., 2008. Micromechanical elastoplastic damage modeling of progressive interfacial arc debonding for fiber reinforced composites. Int. J. Damage Mech. 17, 307–356.
Ju, J.W., Lee, H.K., 2000. A micromechanical damage model for effective elastoplastic behavior of ductile matrix composites considering evolutionary complete particle debonding. Comput. Method Appl. Mech. Eng. 183, 201–222.
Ju, J.W., Lee, H.K., 2001. Micromechanical damage model for effective elastoplastic behavior of partially debonded ductile matrix composites. Int. J. Solids Struct. 38, 6307–6332.
Ju, J.W., Sun, L.Z., 2001. Effective elastoplastic behavior of metal matrix composites containing randomly located aligned spheroidal inhomogeneities. Part I: micromechanics-based formulation. Int. J. Solids Struct. 38, 183–201.
Ju, J.W., Tseng, K.H., 1996. Effective elastoplastic behavior of two-phase ductile matrix composites: a micromechanical framework. Int. J. Solids Struct. 33, 4267–4291.
Ju, J.W., Zhang, X.D., 2001. Effective elastoplastic behavior of ductile matrix composites containing randomly located aligned circular fibers. Int. J. Solids Struct. 38, 4045–4069.
Khan, A.S., Huang, S.J., 1995. Continuum Theory of Plasticity. Wiley, New York.

Khan, A.S., Chen, X., Abdel-Karim, M., 2007. Cyclic multiaxial and shear finite deformation response of OFHC: part I, experimental results. Int. J. Plasticity 23, 1285–1306.

Kim, B.R., Lee, H.K., 2009. An RVE-based micromechanical analysis of fiber-reinforced composites considering fiber size dependency. Compos. Struct. 90, 418–427.

Lee, H.K., Pyo, S.H., 2008. An elastoplastic multi-level damage model for ductile matrix composites considering evolutionary weakened interface. Int. J. Solids Struct. 45, 1614–1631.

Lee, H.K., Simunovic, S., 2001. A damage constitutive model of progressive debonding in aligned discontinuous fiber composites. Int. J. Solids Struct. 38, 875–895.

Li, D.S., Wisnom, M.R., 1996. Micromechanical modelling of SCS-6 fibre reinforced Ti–6Al–4V under transverse tension-Effect of fibre coating. J. Compos. Mater. 30, 561–588.

Li, S., Sauer, R.A., Wang, G., 2005. A circular inclusions in a finite domain I. The Dirichlet-Eshelby problem. Acta Mech. 179, 67–90.

Li, S., Ghosh, S., 2007. Modeling interfacial debonding and matrix cracking in fiber reinforced composites by the extended Voronoi cell FEM. Finite Elem. Anal. Des. 43, 397–410.

Lubliner, J., 1990. Plasticity Theory. Macmillan, New York.

Majumdar, B.S., Newaz, G.M., 1992. Inelastic deformation of metal matrix composites: plasticity and damage mechanisms. Philos. Mag. A66, 187–212.

Meraghni, F., Blakeman, C.J., Benzeggagh, M.L., 1996. Effect of interfacial decohesion on stiffness reduction in a random discontinuous-fibre composite containing matrix microcracks. Compos. Sci. Technol. 56, 541–555.

Moreo, P., García-Aznar, J.M., Doblaré, M., 2007. A coupled viscoplastic rate-dependent damage model for the simulation of fatigue failure of cement-bone interfaces. Int. J. Plasticity 23, 2058–2084.

Nimmer, R.P., Bankert, R.J., Russell, E.S., Smith, G.A., Wright, P.K., 1991. Micromechanical modeling of fiber/matrix interface effects in transversely loaded SiC/Ti-6-4 metal matrix composites. J. Compos. Tech. Res. 13, 3–13.

Oleszkiewicz, E., Łodygowski, T. 2006. Analysis of metal matrix composites damage under transverse loading. In: Sadowski, T. (Ed.), IUTAM Symposium on Multiscale Modelling of Damage and Fracture Processes in Composite Materials 89-96, Springer, Printed in the Netherlands.

Simo, J.C., 1998. Topics on the numerical analysis and simulation of plasticity. In: Ciarlet, P.G., Lions, J.L. (Eds.), Handbook of Numerical Analysis III. Elsevier Science Publishers/North Holland, Amsterdam.

Simo, J.C., Hughes, T.J.R., 1998. Computational Inelasticity. Springer-Verlag, New York.

Sun, C.T., Chen, F.J.L., Sha, G.T., Koop, W.E., 1990. Mechanical characterization of SCS-6/Ti-6-4 metal matrix composites. J. Compos. Mater. 24, 1029–1059.

Tohgo, K., Weng, G.J., 1994. A progress damage mechanics in particle-reinforced metal-matrix composites under high triaxial tension. J. Eng. Mater. Technol. 116, 414–420.

Wang, G., Li, S., Sauer, R.A., 2005. A circular inclusions in a finite domain II. The Neumann-Eshelby problem. Acta Mech. 179, 91–110.

Weibull, W., 1951. A statistical distribution function of wide applicability. J. Appl. Mech. 18, 293–297.

Whitehouse, A.F., Clyne, T.W., 1993. Cavity formulation during tensile straining of particle and short fiber metal-matrix composites. Acta Metall. Mater. 41, 1701–1711.

Zhao, Y.H., Weng, G.J., 1996. Plasticity of a two-phase composite with partially debonded inclusions. Int. J. Plasticity 12, 781–804.

Zhao, Y.H., Weng, G.J., 1997. Transversely isotropic moduli of two partially debonded composites. Int. J. Solids Struct. 34, 493–507.